Structure Sensitivity in the Electrocatalytic Reduction of CO_2 with Gold Catalysts

Mezzavilla, Stefano; Horch, Sebastian; Stephens, Ifan; Seger, Brian; Chorkendorff, Ib

Published in:
Angewandte Chemie International Edition

Link to article, DOI:
10.1002/anie.201811422

Publication date:
2019

Document Version
Peer reviewed version

Structure Sensitivity in the Electrocatalytic Reduction of CO_2 with Gold Catalysts

Stefano Mezzavilla[a],†, Sebastian Horch[a], Ifan E.L. Stephens[a],[b], Brian Seger[a], Ib Chorkendorff[a]*

[a] Dr. S. Mezzavilla, Prof. Dr.S. Horch, Prof. Dr. I.E.L. Stephens, Prof. Dr. B. Seger, Prof. Dr. I. Chorkendorff
SurfCat, Department of Physics,
Technical University of Denmark, DK-2800 Kgs. Lyngby, Denmark
[b] Prof. Dr. I.E.L. Stephens
Department of Materials,
Imperial College London, Royal School of Mines London SW72AZ, England

*Corresponding author E-mail: ibchork@fysik.dtu.dk

† Current address:
Department of Materials,
Imperial College London, Royal School of Mines London SW72AZ, England

Abstract: The understanding of how structural surface features influence electrocatalytic reactions is vital for the development of efficient nanostructured catalysts. Gold is the most active and selective known electrocatalyst for the reduction of CO_2 to CO in aqueous electrolytes. Numerous strategies have been proposed to improve its intrinsic activity. Nonetheless, the atomistic knowledge of the nature of the active sites remains elusive. In this work, we systematically investigated the structure sensitivity for the electrocatalytic CO_2 reduction with Au single crystals. Reaction kinetics for the formation of CO were strongly dependent on the surface structure: under-coordinated sites, such as the ones present in Au(110) and at the steps of Au(211), show at least 20-fold higher activity than more coordinated configurations (e.g. Au(100)). By selectively poisoning under-coordinated sites with Pb, we confirmed that these are the active sites for CO_2 reduction.

The electrocatalytic reduction of CO_2 to CO, hydrocarbons and oxygenates is a promising strategy to convert CO_2 into valuable chemicals using renewable energy sources.[1–3] Gold is the most active electrocatalyst for CO evolution: it has excellent selectivity at low overpotentials in aqueous electrolytes.[4,5] Many strategies, such as alloying,[6] nanostructuring[7,8] and grafting with organic ligands[9] have been proposed to further enhance its performance. Despite these efforts – once geometrical surface area effects are accounted for – polycrystalline gold remains the benchmark catalyst and few systems, if any, have surpassed its intrinsic catalytic activity.[5,10]
Thus far, we have lacked the crucial evidence for how the atomic structure of Au surfaces controls CO_2 reduction.[11] Computational studies predict surface steps to exhibit significantly lower free energy barriers (in comparison to (111) and (100) surfaces) for the formation of the crucial reaction intermediate both for Au and Ag surfaces.[12–15] However, the identity of the active sites remains thus far, experimentally undetermined. Until now, insight on the structure sensitivity for CO_2 electroreduction has rested on investigations of high surface area Au electrodes having varying populations of certain catalytic sites. Kanan and co-workers highlighted how the sites located at grain boundaries are significantly more active than other sites.[16,17] More canonical strategies involve the characterization of nanostructured catalysts with varying sizes or geometries.[18,19] Here, the relative abundance of specific surface defects is often assumed on the basis of geometrical considerations (e.g. particle size). Moreover, given the high surface area nature of these catalysts, it is challenging to disentangle intrinsic structural contributions from surface roughness effects.
Single crystals are ideal systems to identify structure–activity relationships in (electro)catalysis. Their well-defined surface features enable the possibility to probe the contribution of specific surface sites.[11,20,21] Examples are the selective poisoning experiments with Au-doped Ru catalysts for the N_2 dissociation reaction and with Bi-doped Pt single crystal studies for formic acid electro-oxidation.[22] In the context of this work, notable is the insight obtained with Ag crystals by Hori et al. for the electrocatalytic reduction of CO_2 to CO.[23] To the best of our knowledge, gold single crystals have never been studied for the electrocatalytic CO_2 reduction in aqueous electrolytes.
Herein, we probe the role of surface sites in controlling the electrocatalytic reduction of CO_2 on Au. We compare flat (111) and (100) terraces to more open (110) and stepped (211) surfaces. We further investigated the intrinsic activity of defects and steps sites via selective poisoning experiments.
CO_2 electrolysis experiments with Au single crystals (Au*(hkl)*) and polycrystalline Au (pcAu) electrodes were carried out in a temperature-controlled cell at 25 °C in a CO_2 saturated 0.1 M $KHCO_3$ electrolyte (Figure S1). The quality of the crystals was monitored via electrochemical methods and via scanning tunnel microscopy (STM, Figure S3 and S4). CO_2 electrolysis tests were carried out at -0.6 V_{RHE}, -0.7 V_{RHE} and -0.8 V_{RHE}. The crystals were put in

contact with the electrolyte under potential control at 0.1 V_{RHE} and positioned in a hanging meniscus configuration. The electrolyte was constantly purged with CO_2 and mass transfer losses were minimized by stirring the electrolyte (see also discussion in the SI). Prior to the electrolysis tests, the crystals were kept cathodic to the potential at which the reconstruction can be electrochemically lifted.[24] It is therefore safe to assume that the thermally induced surface reconstruction is present under CO_2 electrolysis.[25] STM images taken before/after reaction confirmed that the surface reconstruction and the overall quality of the Au(111) terraces are largely preserved (Figure S4). The concentration of $CHOO^-$, a known minor product of the reaction,[4] was below the analytical detection limits and it was not quantified. Figure 1 reports the partial current densities for CO and H_2 evolution (numerical values in Table S1). Figure 1a reveals a significant structure sensitivity for CO production. The CO partial current density (j_{CO}) registered with Au(110) and Au(211)) is ~20-fold higher than the one measured with Au(100). At -0.6 V_{RHE}, for instance, j_{CO} for Au(110) and Au(211) is 3.05 ± 0.08 and 3.30 ± 0.15 $mAcm_{Au}^{-2}$, respectively, while for Au(100) is 0.14 ± 0.04 $mAcm_{Au}^{-2}$. Au(111) is about 7-fold less active than Au(211). If the rates are normalized to the electrochemical surface area, j_{CO} of pcAu lies between the activity of the Au(110) and Au(111).

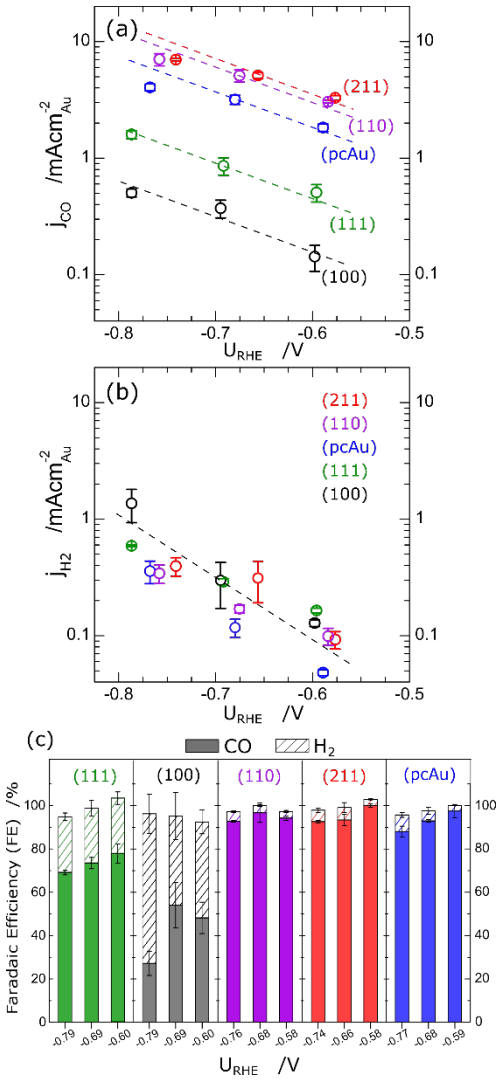

Figure 1. CO_2 electrolysis with Au*(hkl)* and polycrystalline gold (pcAu). (a) CO and (b) H_2 partial current densities normalized to the catalytic surface area. electrolyte: CO_2 saturated 0.1M $KHCO_3$, duration = 1000s; (c) Corresponding faradaic efficiency. The actual measuring potential (after 100% Ohmic correction) is indicated at the bottom of each column

Notably, the pronounced structure sensitivity for CO evolution is not mirrored by a similar trend for the H_2 partial current density (j_{H2}): j_{H2} is similar for all the catalysts irrespective of their surface structure. This results in a significant variation in selectivity between the crystals: while Au(110) and Au(211) reach CO selectivity above 90%, Au(111) and Au(100) show selectivity of ~75% and ~50%, respectively. In agreement with literature result, pcAu

has an intermediate selectivity of ~85%.[4,10] At high overpotentials the selectivity to CO drops for all the crystals; however, notably, at -1 V_{RHE} (Figure S6) Au(110) is still ~80% selective towards CO, while Au(100) produce mostly H_2 (FE for CO is ~13%). These results suggest a correlation between CO evolution kinetics and surface coordination numbers (CN). Surface sites with the highest CN, such as Au(111) and Au(100) (CN of 9 and 8, respectively), are less active than relatively under-coordinated configurations: the top layer of Au(110) and step sites of Au(211) have both CN 7. The impact of the CN on the adsorption energies and on scaling relations has been generalized via DFT.[26]

The relatively weak structure sensitivity for the hydrogen evolution reaction (HER) was confirmed by testing the crystals in phosphate buffer (pH 7), 0.1 M KOH and 0.1M $HClO_4$ in the absence of CO_2 (Figure 2 and Figure S7).

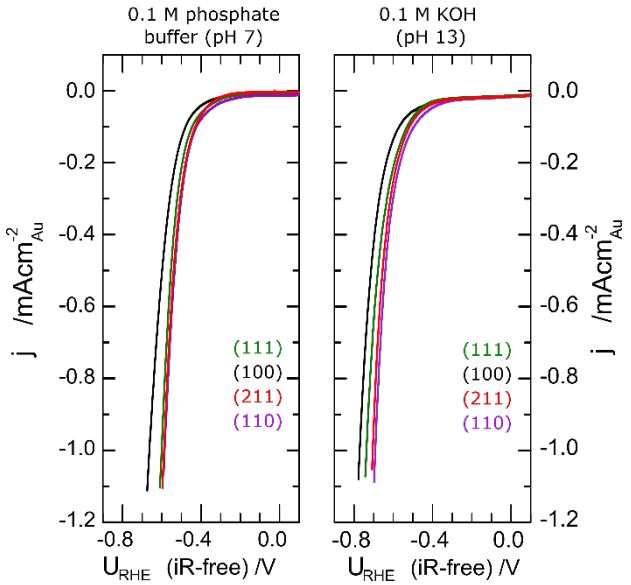

Figure 2. Linear sweep voltammetry curves recorded in H_2 saturated (a) 0.1 M phosphate buffer (pH 7) and (b) 0.1 M KOH with Au(*hkl*). Scan rate = 20 mVs^{-1}, 100 % Ohmic drop corrected.

A thorough discussion of the HER results is reported in the SI. Through the parallel analysis of the CO_2 electrolysis results and HER tests, it is interesting to note how the catalysts most active for CO evolution display the highest rates for the H_2 evolution *per se*. This suggests that H_2O and CO_2 compete for the same sites under CO_2 reduction conditions, with the activation of CO_2 being energetically preferred. Even the most carefully prepared single crystals have a significant proportion of defects, which may still play a dominant role in the reaction. To confirm this hypothesis, controlled amounts of Pb were selectively deposited via Pb under potential deposition (Pb-UPD) on under-coordinated sites to block catalytic events and gauge their effective contribution. Pb-UPD on Au*(hkl)* is known to be very sensitive to the nature of the Au surface.[27–29] Figure 3 shows the Pb-UPD deposition curves for Au(*hkl*) and pcAu as recorded in 0.01 M $HClO_4$ containing 1mM $Pb(ClO_4)_2$ (see Figure S3 for the complete curves). The Pb-UPD deposition on Au(111) presents a double feature at ~0.05 V_{SHE}, which is mirrored by a symmetric peak in the anodic branch (see Figure S3). This peak is assigned to the nucleation and growth of Pb islands on the Au(111) terraces.[29,30] The small convoluted shoulder anodic of the main peak (dashed line in Figure 3) is typically ascribed to the deposition of Pb at the edges of the terraces and at surface defects.[27,29,31] In situ scanning probe microscopy studies suggest that the Pb over-layer on Au(111) nucleates at the edges of the terraces and expands to the terraces resulting in an incommensurate hexagonally closed packed (*hcp*) over-layer.[29,30,32,33]. The adsorption at defects, possibly accompanied by surface alloying phenomena,[32] is highly irreversible, as confirmed by cyclic voltammetry (Figure S3 and S10). In stark contrast, the Pb-UPD curve of Au(110) shows only one peak at ~0.25 V_{SHE}. The Au(211) electrode presents one peak in the same region, ascribed to Pb adsorption at the steps, while the peak at ~0.05 V_{SHE} is assigned to the deposition on the (111) terraces.[28] Although nominally the Au (211) surface is composed of three (111) atomic rows interrupted by monoatomic (100)-type steps, we cannot exclude the flame annealing preparation causes a partial reconstruction towards a more thermodynamic stable (i.e., wider (111) terraces) configuration. As expected, the Pb-UPD deposition profile for pcAu is less defined: the two major

peaks are ascribed to (211)/(110)-types sites (peak at ~0.25 V_{SHE}) and to (111)-type sites (peak at ~0.05 V_{SHE}). The total deposition charge for pcAu (492 μCcm^{-2}) corresponds to a roughness factor of ~1.7 (Table S2). Collectively, Pb-UPD allows us to clearly distinguish the (211)/(110)-type surface sites from (111)-like surfaces.

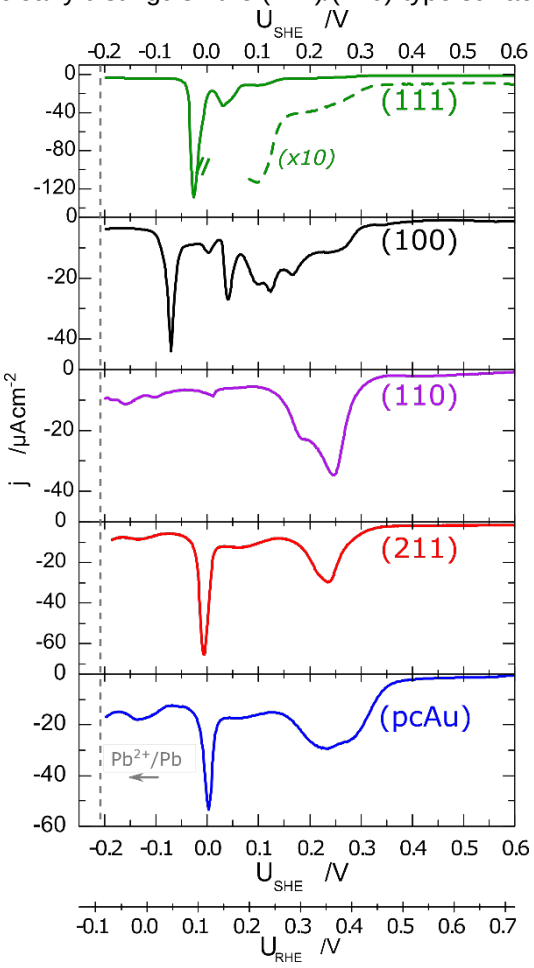

Figure 3. Pb under potential deposition (Pb-UPD) curves for Au(*hkl*) and polycrystalline Au (pcAu) in 0.01 M $HClO_4$ containing 1mM of $Pb(ClO_4)_2$, scan rate = 20 mVs^{-1}. The dashed line indicates the Pb^{2+}/Pb equilibrium potential. See Figure S3 for anodic branches

The poisoning experiments were conducted using a custom-made cell (Figure S2 and related text).[34] Pb was selectively deposited on steps and under-coordinated sites and the blocked surfaces were subsequently tested for CO_2 electrolysis without losing potential control or exposing the electrode to air. Once the excess of Pb^{2+} ions was removed under potential control and the electrolyte was exchanged to CO_2 saturated 0.1M $KHCO_3$, CO_2 electrolysis tests at -0.7 V_{RHE} were initiated. A thorough cleaning procedure was repeated after each experiment to restore the initial state of the surface. All the quality control measures we had in place did not indicate that we altered the nature of the surface with Pb experiments. The full experimental procedure is detailed in the SI file (section S6).
Figure 4 collects the results obtained with pcAu and Au(111). In the Pb poisoning experiments, the UPD was stopped at the initial stages of the deposition before the formation of a full Pb monolayer. More specifically, we stopped the deposition at 0.255 V_{SHE} (experiment P1) and at 0.120 V_{SHE} (experiment P2). For pcAu, the resulting coverages are 21 % and 55 % of a Pb monolayer for experiment P1 and P2, respectively. A third set of experiments was carried out with a full Pb monolayer (Figure S8). For a series of tests, stripping scans were performed as control experiments after the electrolyte exchange to demonstrate the degree of control on the deposition process and to verify the removal of excess Pb^{2+} ions from the electrolyte (dashed lines in Figure 4a). The anodic peak observed for each experiment matches the corresponding deposition curve, indicating that only the fraction of surface sites assigned to (211)/(110)-like sites was covered with Pb. The successful removal of excess Pb^{2+} ions was further confirmed by cyclic voltammetry (Figure S9). Figure 4b shows the results obtained with Pb-blocked surfaces. Because of the small volume of the working electrode compartment, no stirring of the electrolyte nor CO_2 purging was possible during these CO_2 electrolysis experiments. Blank CO2 electrolysis experiments were carried

out with Au electrodes without any Pb (Pb-free): these tests serve as the best comparison as the same mass-transfer conditions apply to Pb-free and Pb-poisoned samples. Remarkably, when the (211)/(110)-type sites are blocked by Pb (experiment P2) j_{CO} decreases from 2.60 mAcm^{-2} to 0.1 mAcm^{-2} (a 20-fold drop compared to the Pb-free electrode). In contrast, j_{H2} remains largely unchanged as it decreases from 0.28 mAcm^{-2} (Pb-free) to 0.14 mAcm-2. A detectable amount of CHOO- is observed (0.12 mAcm-2, 23% FE) for experiment P2. In presence of a full Pb monolayer (Figure S8), the total current density drops to 0.16 mAcm-2, with minute amounts of CO, H2 and CHOO- being formed (approaching the sensitivity limits of the analytical tools). Apart from yielding small amounts of CHOO- (known product of CO2 electrolysis with Pb-based electrodes[35]), at -0.7 VRHE Pb acts as an inert poisoning species. In all the experiments the charge balance reaches ~80%. The remaining 20 % loss is ascribed to (i) the presence of gas products trapped in stagnant corners within the glass cell and (ii) the oxidation of CHOO- at the counter electrode.

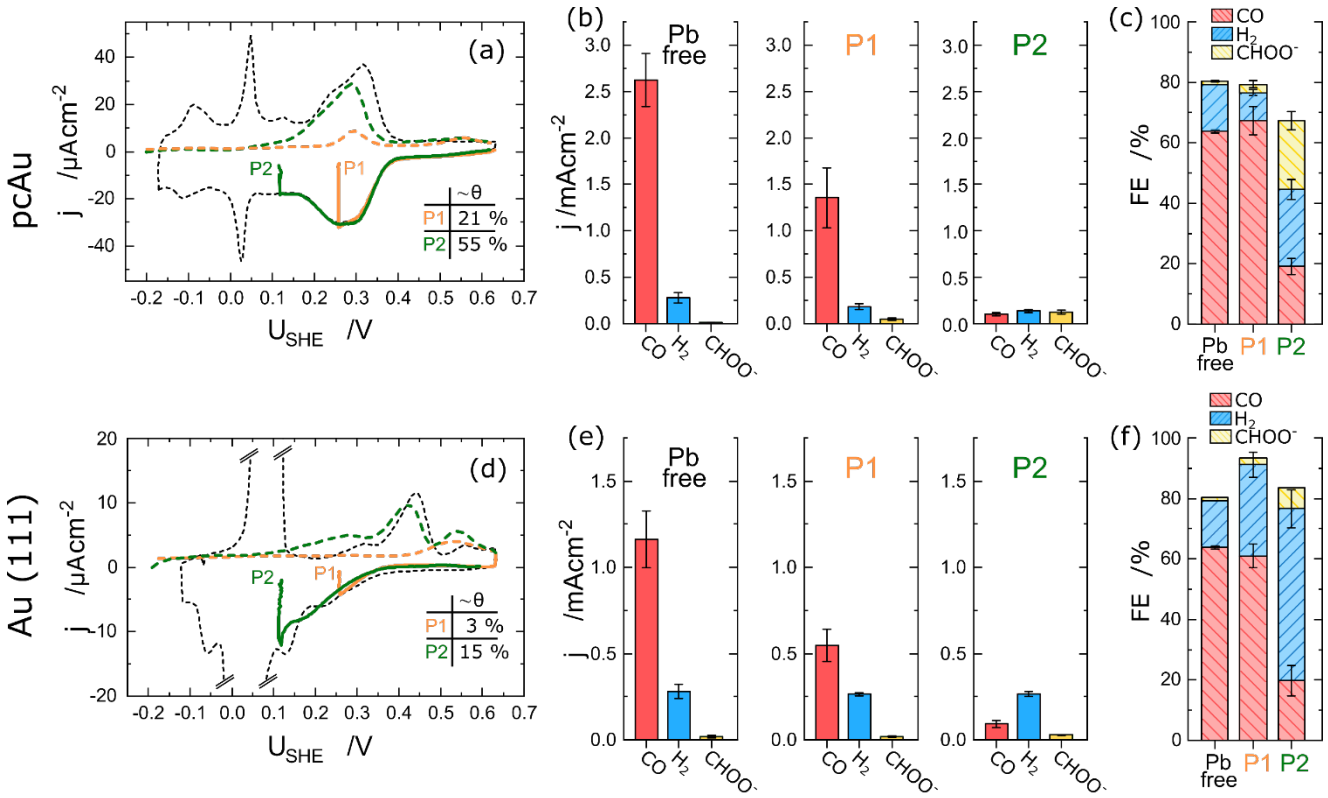

Figure 4. Selective Pb-poisoning experiments with pcAu (upper panel) and Au(111) (lower panel). (a) and (d) Cyclic voltammetry showing the full Pb-UPD curve recorded in 0.01 M $KClO_4$ containing 1mM $Pb(ClO_4)_2$ (black dashed lines), the deposition curves (solid lines) for P1 and P2 and the corresponding stripping curves (dashed lines, colour-coded). The coverage (%) is reported in the inset table. Plot (d) is magnified to make the small features of the cyclic voltammograms visible. (b) and (e) CO, H_2 and $CHOO^-$ partial current densities measured at -0.7 V_{RHE} in CO_2 sat. 0.1 M $KHCO_3$ for the Pb-free surface (left) and for experiments P1 and P2 (c) and (f) Corresponding faradaic efficiencies.

The same set of experiments was carried out with Au(111). Here the goal is to elucidate the role of the defects (e.g., terrace edges) inherently present even on crystals of high quality. By stopping the UPD at its initial stage (shoulder of the main peak), it is possible to selectively cover the surface sites in proximity of terrace edges. The deposition on Au(111) results in much lower Pb coverages: ~3% and ~15% of a Pb monolayer for P1 and P2, respectively. This is expected due to the significantly reduced density of terrace edges and surface defects present on Au(111) compared to pcAu. Control stripping experiments confirm that the Pb was deposited only at the targeted defect sites: only the small stripping features at anodic potentials are visible in Figure 4d. When ~3% of the surface is covered by Pb, the j_{CO} decreases from 1.1 $mAcm^{-2}$ to 0.55 $mAcm^{-2}$ (experiment P1 in Figure 4e), while with 15% of Pb coverage j_{CO} drops to 0.09 $mAcm^{-2}$, which is a factor of 10 less compared to the Pb-free surface. Remarkably, j_{H2} remains constant (~0.28 $mAcm^{-2}$) irrespective of the amount of Pb present on the surface. These results confirm the pronounced structure sensitivity in the CO evolution reaction and suggest that the CO evolution kinetics on surfaces with high coordination numbers, such as Au(111) and Au(100), is likely to be dominated by the small fraction of defects inherently present also on these crystals. The dominance of steps sites – with up to four orders of magnitude higher kinetics than terraces – has been suggested by *ab initio* kinetic models for CO reduction with ideal copper surfaces.[36] To our knowledge, a comparable model for CO evolving catalysts has not yet been reported.

In summary, our results indicate that the electrocatalytic reduction of CO_2 to CO on gold electrodes is remarkably structure sensitive. Catalytic turnover events take place predominantly at under-coordinated sites, thus making the Au(110) and steps-rich surfaces, such and Au(211), at least 20-fold more active than relatively more coordinated surface configurations (e.g. Au(100)). We stress how the selective-blocking strategy may be applied to other substrates and other reactions. We anticipate these findings will offer important elements to optimize the theoretical description of the electrochemical interface. Most importantly, they set the target (i.e., high density of under-coordinated sites) for the synthesis of efficient nanostructured CO evolving catalysts.

Experimental Section

The experimental details for the preparation of the electrodes, for CO_2 electrolysis experiments and the Pb poisoning tests are given in the Supplementary Information file. The raw experimental dataset is deposited in Zenodo: https://doi.org/10.5281/zenodo.154643

Acknowledgements

This project has received funding from the European Union's Horizon 2020 research programme under the Marie Skłodowska-Curie grant agreement No. 705230. The support from the VILLUM Center for Science of Sustainable Fuels and Chemicals funded by the VILLUM Fonden research grant (9455) is also acknowledged.

Keywords: CO_2 electrolysis • gold • single crystals • structure-sensitivity • poisoning

References

[1] N. S. Lewis, D. G. Nocera, *Proceedings of the National Academy of Sciences* **2006**, *103*, 15729–15735.
[2] Z. W. Seh, J. Kibsgaard, C. F. Dickens, I. Chorkendorff, J. K. Nørskov, T. F. Jaramillo, *Science* **2017**, *355*, eaad4998.
[3] T. Haas, R. Krause, R. Weber, M. Demler, G. Schmid, *Nature Catalysis* **2018**, *1*, 32–39.
[4] Y. Hori, A. Murata, K. Kikuchi, S. Suzuki, *Journal of the Chemical Society, Chemical Communications* **1987**, 728.
[5] S. Zhao, R. Jin, R. Jin, *ACS Energy Letters* **2018**, *3*, 452–462.
[6] J. He, N. J. J. Johnson, A. Huang, C. P. Berlinguette, *ChemSusChem* **2018**, *11*, 48–57.
[7] W. Zhu, Y.-J. Zhang, H. Zhang, H. Lv, Q. Li, R. Michalsky, A. A. Peterson, S. Sun, *Journal of the American Chemical Society* **2014**, *136*, 16132–16135.
[8] Y. Chen, C. W. Li, M. W. Kanan, *Journal of the American Chemical Society* **2012**, *134*, 19969–19972.
[9] Y. Fang, J. C. Flake, *Journal of the American Chemical Society* **2017**, *139*, 3399–3405.
[10] Z. P. Jovanov, H. A. Hansen, A. S. Varela, P. Malacrida, A. A. Peterson, J. K. Nørskov, I. E. L. Stephens, I. Chorkendorff, *Journal of Catalysis* **2016**, *343*, 215–231.
[11] A. Kolodziej, P. Rodriguez, A. Cuesta, in *Energy and Environment Series* (Eds.: F. Marken, D. Fermin), Royal Society Of Chemistry, Cambridge, **2018**, pp. 88–110.
[12] S. Back, M. S. Yeom, Y. Jung, *ACS Catalysis* **2015**, *5*, 5089–5096.
[13] J. Rosen, G. S. Hutchings, Q. Lu, S. Rivera, Y. Zhou, D. G. Vlachos, F. Jiao, *ACS Catalysis* **2015**, *5*, 4293–4299.
[14] C. Shi, H. A. Hansen, A. C. Lausche, J. K. Nørskov, *Physical Chemistry Chemical Physics* **2014**, *16*, 4720.
[15] M. R. Singh, J. D. Goodpaster, A. Z. Weber, M. Head-Gordon, A. T. Bell, *Proceedings of the National Academy of Sciences* **2017**, *114*, E8812–E8821.
[16] R. G. Mariano, K. McKelvey, H. S. White, M. W. Kanan, *Science* **2017**, *358*, 1187–1192.
[17] X. Feng, K. Jiang, S. Fan, M. W. Kanan, *Journal of the American Chemical Society* **2015**, *137*, 4606–4609.
[18] W. Zhu, Y.-J. Zhang, H. Zhang, H. Lv, Q. Li, R. Michalsky, A. A. Peterson, S. Sun, *Journal of the American Chemical Society* **2014**, *136*, 16132–16135.

[19] H. Mistry, R. Reske, Z. Zeng, Z.-J. Zhao, J. Greeley, P. Strasser, B. R. Cuenya, *Journal of the American Chemical Society* **2014**, *136*, 16473–16476.
[20] J. K. Nørskov, T. Bligaard, B. Hvolbæk, F. Abild-Pedersen, I. Chorkendorff, C. H. Christensen, *Chemical Society Reviews* **2008**, *37*, 2163.
[21] P. Rodriguez, Y. Kwon, M. T. M. Koper, *Nature Chemistry* **2011**, *4*, 177–182.
[22] M. Maciá, *Electrochemistry Communications* **1999**, *1*, 87–89.
[23] N. Hoshi, M. Kato, Y. Hori, *Journal of electroanalytical chemistry* **1997**, *440*, 283–286.
[24] L. A. Kibler, *International Society of Electrochemistry* **2003**.
[25] D. Kolb, *Progress in Surface Science* **1996**, *51*, 109–173.
[26] F. Calle-Vallejo, D. Loffreda, M. T. M. Koper, P. Sautet, *Nature Chemistry* **2015**, *7*, 403–410.
[27] A. Hamelin, *Journal of Electroanalytical Chemistry and Interfacial Electrochemistry* **1984**, *165*, 167–180.
[28] A. Hamelin, J. Lipkowski, *Journal of electroanalytical chemistry and interfacial electrochemistry* **1984**, *171*, 317–330.
[29] E. Herrero, L. J. Buller, H. D. Abruña, *Chemical Reviews* **2001**, *101*, 1897–1930.
[30] M. P. Green, K. J. Hanson, R. Carr, I. Lindau, *Journal of The Electrochemical Society* **1990**, *137*, 3493–3498.
[31] J. W. Schultze, D. Dickertmann, *Surface Science* **1976**, *54*, 489–505.
[32] M. P. Green, K. J. Hanson, *Surface Science Letters* **1991**, *259*, L743–L749.
[33] C. H. Chen, N. Washburn, A. A. Gewirth, *The Journal of Physical Chemistry* **1993**, *97*, 9754–9760.
[34] A. S. Varela, C. Schlaup, Z. P. Jovanov, P. Malacrida, S. Horch, I. E. L. Stephens, I. Chorkendorff, *The Journal of Physical Chemistry C* **2013**, *117*, 20500–20508.
[35] Y. Hori, H. Wakebe, T. Tsukamoto, O. Koga, *Electrochimica Acta* **1994**, *39*, 1833–1839.
[36] X. Liu, J. Xiao, H. Peng, X. Hong, K. Chan, J. K. Nørskov, *Nature Communications* **2017**, *8*, 15438.